Atomic and electronic structure of polar Fe₂O₃(0001)/MgO(111) interfaces

K. Pande, M. Gajdardziska-Josifovska, and M. Weinert

Department of Physics and Laboratory for Surface Studies, University of Wisconsin-Milwaukee, Milwaukee, Wisconsin 53211, USA
(Received 3 June 2012; published 19 July 2012)

We present a first-principles investigation of the structural, electronic, and magnetic properties of ultrathin Fe₂O₃(0001) films on a polar MgO(111) substrate. The results imply that the heterointerface is atomically abrupt with oxidelike stacking for film thicknesses between ∼1.5 and 8.5 Å. The Fe-Fe bilayer (nominal separation of 0.59 Å in Fe₂O₃) at the interface collapses into an "Fe₂" monolayer. Both electronic polarization and structural relaxations effectively screen the dipole field of the polar interface system. The structural relaxations—consisting of interpenetration, separation, and merger of Fe and oxygen planes—are particularly drastic in the three- and four-bilayers-thick films, giving rise to barrierless movement of oxygen towards the surface and the formation of an "Fe₂|FeO₃" layer structure not seen in hematite. Comparisons to calculations of unsupported polar Fe₂O₃(0001) slabs demonstrate that these unusual changes in stacking sequence and electronic structure are associated with the polar nature of this oxide heterointerface.

I. INTRODUCTION

The polar interfaces between different crystalline oxides (heterointerfaces) are interesting—and controversial—because of their unique local atomic and electronic structure and novel properties.[1–4] For example, in the heterointerface between LaAlO₃/SrTiO₃, which has been extensively studied both experimentally[5–8] and theoretically,[9] the polar discontinuity is accommodated by interface electronic and atomic reconstructions;[10] moreover, by controlling the termination layer at the interface it is possible to have insulating (hole-doped) or conducting (electron-doped) interfaces.[11] Another important class of polar materials are the iron oxides, which are some of the most abundant minerals on Earth and find applications as oxidation catalysts, gas sensors, photonic devices, and magnetic storage media.[12] In studies of the epitaxial growth of Fe₃O₄(111) polar films on polar MgO(111) substrates,[13] the films were found to be stabilized by the formation of Fe nanoparticles in the magnetite film and at the interface. Such phase separation is not observed when polar Fe₃O₄(111) is grown on a metallic Pt(111) substrate.[14] First-principles studies of the Fe₃O₄(111)/MgO(111) heterointerfaces[15] predict metal-induced gap states in the interface oxygen and an energetic preference for an abrupt oxidelike interface initiated with Fe in the octahedral sites.

In this paper we report a first-principles study of the heterointerface between polar magnesia (MgO) substrate and polar hematite (α-Fe₂O₃) ultrathin films in order to probe the effects of substrate polarity on the trends in atomic and electronic structure at the interface. Bulk hematite is an antiferromagnetic insulator that has a polar surface in the ⟨0001⟩ direction. Over the years there have been a number of electronic structure calculations of Fe₂O₃, both for the bulk[16–19] and for the free surface.[20–23] The correlated nature of the Fe 3d electrons, and their role in the structural properties of the iron oxides, has been of interest, particularly in relation to the spectroscopic i.e., band gap data. In spite of this issue, structural properties calculated at the generalized gradient approximation (GGA)[23] and the GGA + U (Ref. 22) level give generally consistent results in broad agreement with the experimental results.

The issues to be addressed here are how, if at all, the polarity of the substrate affects the layer-by-layer growth of the film, the factors that lead to stable films, and the resulting structure at the interface. To distinguish between effects induced by the polar interface from those driven by the polar surface of the film, we compare equivalent unsupported slabs of Fe₂O₃(0001). The calculations for thin Fe₂O₃(0001) films on polar MgO(111) substrates show that the properties of the films are thickness dependent and differ significantly from bulk Fe₂O₃. In particular, we find large structural relaxations in the film that result in changes in the stacking of Fe and O planes, as well as a variety of magnetic configurations. To see if this behavior is unique to the polar heterointerface, we compare model calculations for unsupported Fe₂O₃(0001) polar slabs and find distinct differences in the structure and properties between the slabs and the heterointerfaces. In Sec. II we describe the computational details and the known structure of bulk hematite. Discussions of the results on our model calculations for bulk Fe₂O₃, Fe₂O₃(0001)/MgO(111) polar interface, and unsupported Fe₂O₃(0001) slabs are presented in Sec. III, and concluding remarks and open key questions are discussed in Sec. IV.

II. METHODS AND STRUCTURAL MODELS

α-Fe₂O₃ crystallizes in the corundum structure, space group $R\bar{3}c$, with six formula units in the conventional hexagonal cell (two in the primitive rhombohedral cell), consisting of slightly distorted hexagonal close-packed layers of oxygen ions with two-thirds of the octahedral sites occupied by Fe ions. The stacking sequence along the [0001] direction can be represented as *ABACABAC...* with "bilayers" of Fe atoms in *A* sites (with the "missing" Fe also following a rhombohedral sequence in the three possible *A* sites) and alternating *B* and *C* planes of oxygen as shown in Fig. 1. Fe-Fe nearest neighbors (nn) correspond to Fe atoms between two successive bilayers separated by a layer of oxygen atoms ($d_{nn}^{Fe\text{-}Fe} = 2.86$ Å). The separation between Fe planes in the bilayer is $d_{\perp}^{Fe\text{-}Fe} = 0.59$ Å and between successive Fe and O planes is $d_{\perp}^{Fe\text{-}O} = 0.83$ Å; the Fe-O bond length is $d_{nn}^{Fe\text{-}O} = 1.93$ Å. MgO has a rocksalt
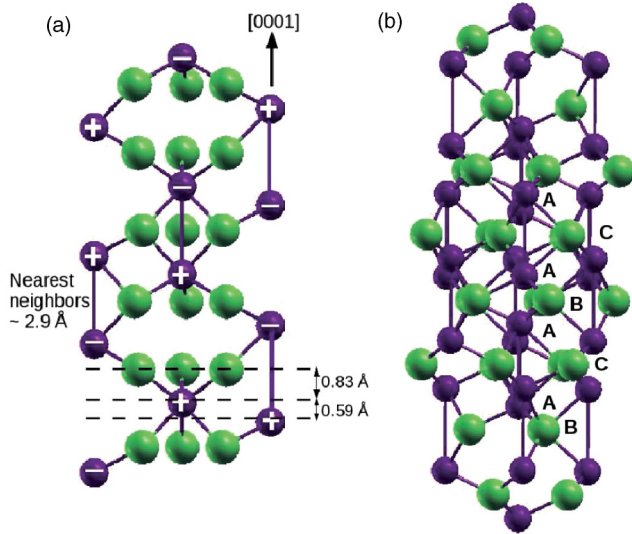
FIG. 1. (Color online) Structure of bulk hexagonal α-Fe$_2$O$_3$. The green (light) and purple (dark) spheres represent the O and Fe atoms, respectively. (a) Bulk unit cell in a $\langle 1\bar{1}00 \rangle$ projection: $+$ and $-$ indicate the relative magnetic ordering of Fe atoms. (b) $\langle 11\bar{2}0 \rangle$ crystal projection showing the *ABAC* stacking sequence with Fe atoms in *A* sites and O atoms alternating between *B* and *C* sites.

TABLE I. Total energies (eV/Fe atom) of different magnetic orderings for bulk α-Fe$_2$O$_3$ as a function of the spin configuration relative to AF$_B$ (antiferromagnetic unit cell with parallel intralayer and antiparallel interlayer Fe moments).

Magnetic ordering	Spin configuration	ΔE
AF$_B$	$++\,\vert -\,-$	0
AF$_I$	$+-\,\vert -\,+$	0.22
AF$_{II}$	$+-\,\vert +\,-$	0.22
FM	$++\,\vert +\,+$	0.32
NM		0.44

structure with an experimental lattice constant of 4.217 Å. The MgO stacking along the [111] direction has alternating Mg and O planes stacked in the characteristic *ABC* fcc stacking. Both Fe$_2$O$_3$ and MgO have hexagonal in-plane symmetry in their polar {0001} and {111} directions. The Fe$_2$O$_3$(0001) unit cell fits well on the $\sqrt{3} \times \sqrt{3}$ 30° rotated MgO lattice with a lattice mismatch of $\sim$3% on the rotated hexagonal plane.

Spin-polarized density functional theory (DFT) calculations were done in a slab geometry using the full-potential linearized augmented plane wave (FLAPW) method[24,25] as implemented in FLAIR.[26] For the majority of the calculations, exchange correlation was treated using the GGA parametrization of Perdew-Burke-Ernzerhof.[27] The Brillouin zone sampling was adjusted to maintain constant density in the reciprocal space, corresponding to $\sim$2500–4000 k points for an equivalent monotonic solid. The wave functions were expanded in spherical harmonics up to $\ell_{max} = 8$ inside the atomic spheres ($R_{Fe,Mg}$=2 bohrs, R_O = 1.33 bohrs). Full structural relaxations (with a convergence criterion of 0.002 eV/Å) and spin reorientations were carried out. Calculations for bulk Fe$_2$O$_3$ were done in a rhombohedral geometry, while those for Fe$_2$O$_3$(0001)/MgO(111) polar interfaces and unsupported Fe$_2$O$_3$(0001) slabs were done in a hexagonal geometry. Heterointerface calculations used symmetric slabs consisting of 11 layers of MgO with Fe-O layers on both sides in order to remove the artificial interslab dipole interactions, and with vacuum separations of $\sim$17–20 Å.

Calculations for bulk rhombohedral Fe$_2$O$_3$ (ten atoms per unit cell) were done for various magnetic configurations, including ferromagnetic (FM) and antiferromagnetic (AF). For the AF ordering, there are three possible local spin configurations: AF$_B$ $(++\,\vert -\,-)$ with spins parallel within each Fe bilayer and antiparallel with the neighboring Fe

bilayers (the experimentally known stable structure); and AF$_I$ $(+-\,\vert -\,+)$ and AF$_{II}$ $(+-\,\vert +\,-)$ with spins antiparallel within each bilayer. (In this notation, the vertical bar separates two successive bilayers and the rightmost spin is for the "upper" atom of the bilayer. The nearest-neighbor Fe atoms correspond to the first and fourth sites, i.e., a "lower" bilayer site and the "upper" site four sites to the right in the sequence are nearest neighbors.) The nearest neighbors are coupled antiferromagnetically in AF$_B$ and AF$_{II}$, but ferromagnetically in AF$_I$. The AF$_B$ configuration with parallel spins within each bilayer is energetically favored (Table I) and yields a lattice constant a = 4.98 Å, 1.1% less than the experimental value of 5.035 Å. The calculated c/a ratio is 2.70, in close agreement with the experimental value of 2.73. Other calculated bulk parameters, such as nearest-neighbor distances, differ from the experimental values by less than 1.2%. The calculated magnetic moment in the Fe spheres was $\sim$3.4μ_B.

Our spin-polarized GGA $+$ U calculations give an equilibrium lattice constant of 5.00 Å (0.8% less than the experimental lattice constant) and a band gap of 2.01 eV for $U - J = 4$. The calculated nearest-neighbor distances are $d_{nn}^{Fe-Fe} = 2.87$ Å and $d_{nn}^{Fe-O} = 1.93$ Å, in reasonable agreement with the experimental values, and vary from the GGA results by only $\sim$1.1%, consistent with previous results. Excited state properties such as band gaps, on the other hand, depend on the value of U, which in turn is strongly dependent on the local environment; i.e., there is no *single* consistent value of U appropriate for metallic Fe, FeO, Fe$_3$O$_4$, and Fe$_2$O$_3$. Because of the ambiguity in the choice of U, especially in this interface environment, and because we are mainly interested in the structural properties, the majority of the calculations have been done at the GGA level. However, in order to assess the robustness of our conclusions, we have also repeated some representative calculations using the GGA $+$ U, and will be discussed in Section III C.

A. Polarity and potential analysis

To both qualitatively and quantitatively address the issues related to polarity, we will present results for the self-consistently calculated planar-averaged Coulomb potentials. The Coulomb potentials, which include all the electronic (and possibly structural) screening effects, provide a firm starting point for making contact with simple models and concepts. In particular, ionicity is an often used concept, even though it is difficult to define uniquely. We have approached the

problem by allowing the ionicity to be a fitting parameter. The superposition of (ionic) atomiclike densities often provides a well-defined reference and a good initial guess for the charge density. The contribution of the ith atom to this overlapped charge density is

$$\rho_i(\vec{r}) = [n_i(\vec{r}) - Z_i\,\delta(\vec{r})] - q_i\,n_i^v(\vec{r}),$$

where n_i is the electronic density of the neutral atom of charge Z_i, q_i is the ionicity, and n_i^v is the density corresponding to a valence electron ($2p$ for O, $3s$ for Mg, and $3d$ for Fe). With this division, the terms in the brackets will generate a planar-averaged Coulomb potential for neutral entities, $V_{\text{neutral}}(z)$, and the second one will generate an "ionic" potential, $V_{\text{ion}}(z; q_i)$ that depends on the individual ionicities. The q_i values are determined by a linear least-squares fit (using a singular value decomposition approach) of

$$V_{\text{ion}}(z; q_i) = V_c(z) - V_{\text{neutral}}(z),$$

where $V_c(z)$ is the self-consistent planar-averaged Coulomb potential. This model takes into account the spatial extent of the different atoms and orbitals, which is essential since $V_{\text{neutral}}(z)$ is generally the largest contribution to the potential.

B. Atomic models for the heterointerface: Fe₂O₃(0001)/MgO(111)

To understand the initial stages of the growth process, calculations were carried out for a series of ultrathin Fe_2O_3 films, for both oxide (...3Mg|3O|Fe-Fe|3O|Fe-Fe...) and metal (...3O|3Mg|Fe-Fe|3O...) interface orderings on oxygen-terminated MgO(111). The thinnest film consisted of a single ($n = 1$) Fe bilayer (with a nominal thickness of 1.48 Å); the $n = 2$–4 Fe-bilayer films added $n - 1$ stoichiometric 3O|Fe-Fe units, for nominal thicknesses of 3.8–8.5 Å. Because we are modeling the initial layer-by-layer growth rather than the equilibrium surface termination, most of the calculations assumed a stoichiometric Fe termination (corresponding to molecular beam epitaxial growth in an Fe flux), although calculations with different initial terminations were also considered. The initial geometries consisted of either $n = 1$–4 bulk hematite units on MgO(111), or the addition of a bulk Fe_2O_3 unit on top of the relaxed structure. (Additional geometries to address issues of lattice mismatches and chemical environment were also considered and are discussed below.)

III. RESULTS AND DISCUSSION

A. Nature of the interface and structural relaxations

As the first Fe atoms adsorb on the MgO(111) surface, the question is whether the interface is oxide-metal or metal-metal. The calculated adhesive energy for the O-terminated substrate, corresponding to Mg-O-Fe ordering at the interface, is more binding by $\sim$0.3 eV/Å^2 than an O-Mg-Fe stacking, confirming the oxide nature of the interface. Interface mixing of Mg(O) and Fe was modeled by forming Fe,Mg(O) antisites for one-third of the interface Mg(O) atoms. The Fe-Mg intermixing is energetically unfavorable, costing $\sim$2 eV/Fe-Mg pair. An interchange of Fe and O results in an unstable interface (the forces on the atoms act to reverse the motion) because the strong ionic Fe-O and Mg-O bonds are replaced by weaker metallic Fe-Mg and covalent O-O bonds. Although interface roughening has been proposed as a possible solution to the polarity problem,[10,28] our calculations suggest that the polar interface between MgO and Fe_2O_3 is atomically abrupt. This observation is supported by high-resolution transmission electron microscopy (HRTEM) images[29] that show abrupt interfaces between the MgO substrate and the hematite film, as well as previous studies of the Fe_3O_4(111)/MgO(111) interface structure.[15]

At all modeled film thicknesses there are noticeable shifts in the atomic positions of the Fe and O atoms in the hematite film (Table II). The film with just one Fe bilayer is stabilized by the complete collapse of the bilayer into a single plane irrespective of the magnetic coupling between the Fe atoms: In the absence of other Fe and O neighbors, both Fe atoms at the surface see the same local environment and there is no driving force to cause a difference in the heights of the different Fe atoms. For the film with two Fe bilayers, there is a large contraction in the interplanar Fe-Fe and Fe-O spacings close to the interface.

The structural relaxations for the $n = 3$ Fe-bilayer case are especially noteworthy. For monolayer Fe termination (only one of the two Fe atoms per bilayer, "3*" in Table II), the surface Fe atom shows an inward relaxation of $\sim$0.74 Å, resulting in a reduction in the interlayer Fe-O separation by 89%, and the interface Fe bilayer has almost collapsed, reducing the interplanar distance to 0.09 Å. The relaxed (half-metallic) film retains the same stacking sequence of Fe and O planes as the unrelaxed film (alternating planes of O and Fe bilayers), albeit stabilized by large intra- and interlayer relaxations. When an

TABLE II. Interplanar distances in Å between Fe planes within an Fe bilayer, and between surface Fe and O planes. The fractional change $\delta \equiv \Delta d/d$ (in %) relative to the intraplanar and interplanar spacings in bulk α-Fe_2O_3 are given in square brackets [ ]; 3* refers to a film terminated with a single Fe atom. The subscripts 1, 2, 3, and 4 refer to the first, second, third, and fourth bilayer from the interface, respectively, and the Fe-O relaxation is for the Fe-O pair at the surface. For comparison, the bulk intralayer distances are $d_\perp^{\text{Fe-Fe}} = 0.59$ Å and $d_\perp^{\text{Fe-O}} = 0.83$ Å. The results are for the most stable spin configuration.

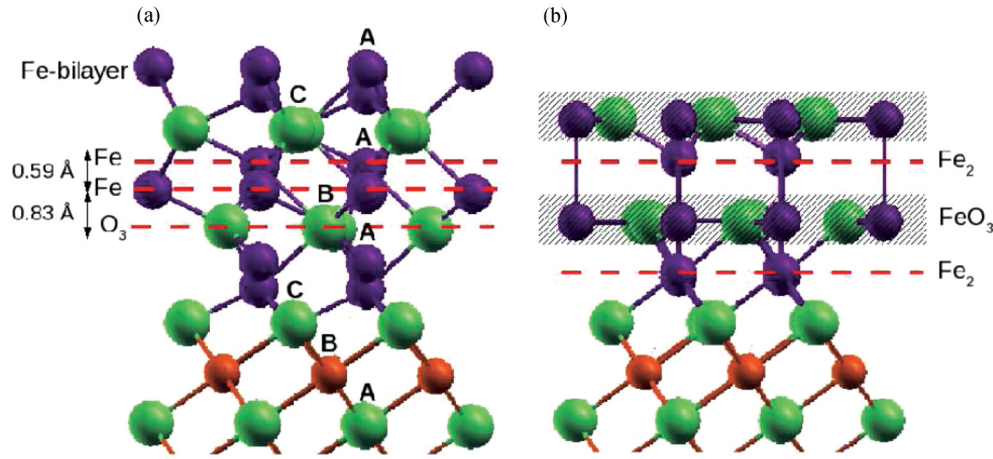| Fe bilayers	$d_{\perp,1}^{\text{Fe-Fe}}[\delta]$	$d_{\perp,2}^{\text{Fe-Fe}}[\delta]$	$d_{\perp,3}^{\text{Fe-Fe}}[\delta]$	$d_{\perp,4}^{\text{Fe-Fe}}[\delta]$	$d_{\perp,s}^{\text{Fe-O}}[\delta]$
1	0.0 [−100]				1.13 [35]
2	0.20 [−66]	0.55 [−6]			0.22 [−73]
3*	0.09 [−85]	0.67 [14]			0.09 [−89]
3	0.02 [−97]	1.60 [170]	0.95 [61]		0.01 [−98]
4	0.26 [−55]	0.78 [32]	1.18 [100]	0.06 [−90]	0.13 [−85]

FIG. 2. (Color online) Side view of the (a) unrelaxed and (b) relaxed structures for the three-Fe-bilayer hematite film on MgO(111). Purple (dark), green (light), and orange (medium dark) spheres represent Fe, O, and Mg, respectively.

additional Fe is added—a complete Fe bilayer is present—drastic changes in structure occur (Fig. 2), resulting in the formation of a relaxed film consisting of $Fe_2|FeO_3$ planes and large changes in interlayer distances. The interplanar distance between relaxed oxygen planes is 2.57 Å, a 9.8% expansion compared to a separation of 2.34 Å for unrelaxed O. The largest change is the 170% (1.11 Å) expansion of the Fe bilayer, which occurs as one of the Fe atoms in the bilayer passes *through* one of the neighboring oxygen planes. (The Fe and O atoms occupy different sites, A vs B/C.)

The final structure is the result of a barrierless set of structural relaxations shown in Fig. 3: Starting from the initial Fe_2O_3 stacking, the subsurface oxygen plane moves outward and one of the Fe atoms in the surface bilayer passes through this O plane. This motion triggers the rearrangement of the

Fe bilayers lying deeper in the film, resulting in the flattening of the interface Fe bilayer into an Fe_2 plane. The coordinated relaxation of the surface and intermediate Fe bilayers seen in Fig. 3 leads to the formation of two FeO_3 planes (with the Fe atoms both in the A_0 site) separated by an Fe_2 plane that has the same local structure (Fe in the A_{-1} and A_1 sites) as the Fe_2 plane at the interface. The film structure on the substrate therefore changes from being $...3Mg|3O|Fe-Fe|3O|Fe-Fe|3O|Fe-Fe$ to $...3Mg|3O|Fe_2|FeO_3|Fe_2|FeO_3$. The effective local Fe-O stoichiometry changes from 2:3 to 1:1, corresponding to oxygen from the inner layer being pushed towards the top of the film. This Fe_2-FeO_3 stacking does not exist in any of the bulk iron oxides found in nature. Constructing a bulklike unit cell with such ordering and the 1:1 stoichiometry results in an antiferromagnetic ground
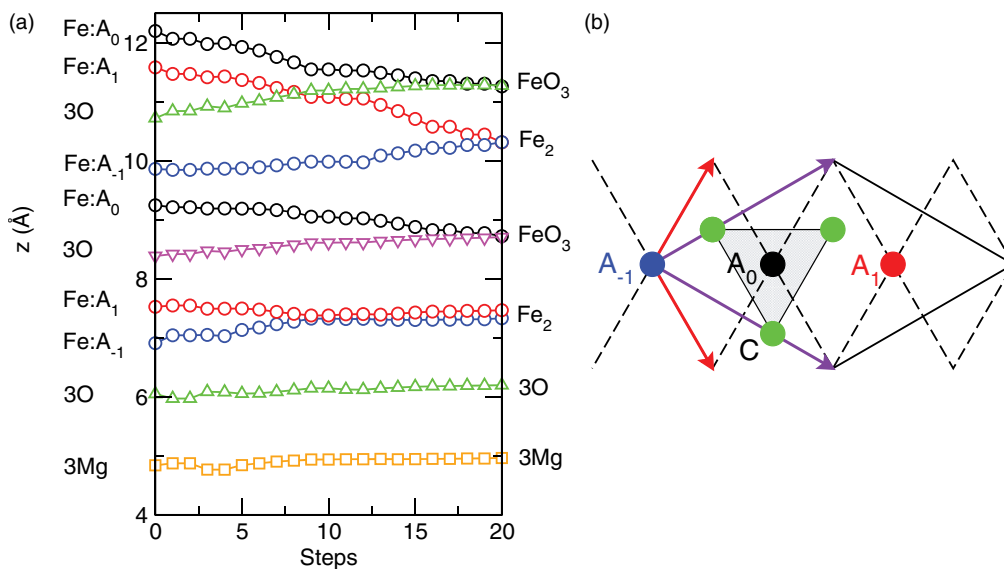

FIG. 3. (Color online) (a) Atomic positions along the surface normal for atoms in the three-bilayer film as a function of the relaxation steps. The in-plane atomic positions are indicated on the left and the final layer structure on the right. (b) Top view of the hexagonal plane. Red and purple arrows represent the (1×1) MgO plane and the $Fe_2O_3(0001)$/MgO(111) $(\sqrt{3} \times \sqrt{3})$ in-plane lattice vectors, respectively. The possible Fe sites (A_{-1}, A_0, A_1) and one set of the oxygen sites (C) are indicated; the shaded gray triangle shows the local structure of the FeO_3 plane.

TABLE III. Interplanar distances in Å for four-Fe-bilayers-thick $Fe_2O_3(0001)/MgO(111)$ films modeled starting from the relaxed structure for three Fe bilayers (the film structure with $FeO_3|Fe_2$ planes) and adding an Fe bilayer (4*) followed by a 3O plane (4**) or a 3(O-Fe-Fe) unit (4†) to simulate a layer-by-layer growth as shown in Fig. 4. Fractional changes in distances $\delta = \Delta d/d$ (in % with respect to distance in bulk Fe_2O_3) are given in square brackets [ ]. For comparison, the starting intralayer distances are $d_\perp^{Fe_2} = 0$ Å, $d_\perp^{FeO_3} = 0$ Å, $d_\perp^{Fe-Fe} = 0.59$ Å, and $d_{\perp,s}^{Fe-O} = 0.83$ Å. Subscripts I and s refer to interface and surface, respectively.

Fe bilayers	$d_{\perp,I}^{Fe_2}[\delta]$	$d_{\perp,I+1}^{FeO_3}[\delta]$	$d_{\perp,I+2}^{Fe_2}[\delta]$	$d_{\perp,I+3}^{FeO_3}[\delta]$	$d_{\perp,s}^{Fe-Fe}[\delta]$	$d_{\perp,s}^{Fe-O}[\delta]$
4*	0.04 [−93]	0.02 [−98]	0.20 [−66]	0.59 [−29]	0.03 [−95]	
4**	0.02 [−97]	0.58 [−30]	0.68 [15]	1.30 [57]	0.48 [−19]	0.30 [−64]
4†	0.05 [−92]	0.63 [−24]	0.31 [−47]	1.33 [60]	0.14 [−76]	0.14 [−83]

state which is ∼0.15 eV/Fe atom less stable than the AFM ground state of FeO. Experimentally, the existence of precursor 1:1 Fe-O phases have been inferred at the initial stages of hematite growth on a variety of substrates, including (polar) α-Al_2O_3,[30–33] metals [Pt(111),[34] Ag(111),[35] Mo(110)[36]], and at the (nonpolar) Fe-MgO(001) interfaces of magnetic tunnel junctions.[37] Although the structures of these various possible Fe-O phases are not known—and hence cannot be directly compared—these experimental observations indicate that the structure of ultrathin Fe-oxide films differs from that of the bulk due to interactions with the substrate, but there is no apparent direct correlation between the polarity (or metallicity) of the substrate and the existence of these FeO phases.

A striking feature of this structural relaxation is that it is independent of the local spin configuration and, more importantly, takes place without an energy barrier. The final structure is similar independent of the starting positions of the Fe and O atoms in the Fe_2O_3 film. Calculations for a three-bilayer film with an O_3 stacking fault show similar rearrangements of the Fe and O atoms forming $Fe_2|FeO_3$ planes, even though the cost of introducing such a stacking fault is ∼0.7 eV/interface. Both structures, with and without a stacking fault, are half metallic (at the GGA level) throughout the film.

The growth of the next O layer and Fe bilayer on the relaxed three-bilayer film was modeled in two different ways: To simulate oxygen-poor conditions the growth was initiated with an Fe bilayer followed by an O plane, while oxygen-rich conditions were mimicked by the addition of a 3O|Fe-Fe unit. The relaxed interplanar distances are given in Table III and the sequence of atomic relaxations is shown in Figs. 4(a) and 4(b), respectively, with the structure in Fig. 4(a) being energetically favorable by ∼0.12 eV/interface.

In an oxygen-poor growth environment, the deposition of an Fe bilayer on the FeO_3 terminated film [Fig. 4(a)] unfolds the FeO_3 plane into Fe and 3O planes, while the surface Fe bilayer collapses into an Fe_2 plane. The deeper layers, however, still maintain their structure. Introduction of oxygen triggers a slight unfolding of the subsurface Fe_2 and FeO_3 planes, but the Fe_2 plane at the interface remains unchanged. The final structure consists of trilayers of Fe between O planes, i.e., an Fe-Fe-Fe|3O structure, with a 1:1 local stoichiometry of Fe and O. Similar unfolding of planes takes place in an oxygen-rich environment, but with a different surface termination, an "Fe_2O_3" termination rather than a 3O termination.

If instead of modeling epitaxial growth, i.e., adding one stoichiometric unit of Fe_2O_3 at a time, we model a four-Fe-bilayers-thick film with the typical hematite Fe-Fe|3O stacking, we obtain a structure that retains the bulk stacking sequence, although still with significant interplanar relaxations (cf. Table II). This structure is energetically more stable (0.14 eV/interface) than the one obtained from the layer-by-layer growth model, as expected since as the Fe_2O_3 film becomes thicker, the bulk structure should become favorable. On the other hand, during (quasiequilibrium) epitaxial growth the structure that forms is a local minimum at that particular stage of growth, and not the global minimum. Kinetics likely also play an important role. These factors taken together imply that the growth may have a strong dependence on experimental conditions and the metastable nature of the structure.

The origin of stability of this higher energy iron oxide phase ($Fe_2|FeO_3$) could be, for example, the low-dimensional constraints of thickness, in-plane lattice constant, or by the polarity contributions of the surface and/or interface. To separate the effects of the polar heterointerface from the surface/bulk contributions, we carried out a systematic study of the structure and properties of unsupported hematite slabs with equivalent thicknesses and initial surface termination. The structure of the polar $Fe_2O_3(0001)$ surface itself remains an open question even after extensive experimental and theoretical studies. For example, spectroscopy studies on α-$Fe_2O_3(0001)$ surfaces grown by oxygen-plasma-assisted molecular beam epitaxy (OPAMBE) have found stable Fe-terminated surfaces.[38] Calculations, on the other hand, have predicted a variety of surface terminations depending on the oxygen partial pressure: At high oxygen chemical potentials, the most stable surface of hematite (0001) is completely covered with oxygen (...Fe-Fe|3O), while at very low chemical potentials a surface with only one iron atom (...Fe-3O|Fe) is stable.[20,22,23] The presence of ferryl-terminated surfaces over a small intermediate domain[1,39] has also been suggested. In the present study, most calculations for the $Fe_2O_3(0001)$ slabs and $Fe_2O_3(0001)/MgO(111)$ interface systems are initiated with Fe-terminated surfaces, which necessarily occur during the layer-by-layer growth of hematite films that is the impetus for our work.

We limit our investigation to α-$Fe_2O_3(0001)$ surfaces with stoichiometric Fe-Fe termination and construct symmetric slabs with thickness varying from three Fe bilayers (eight atomic layers, ∼5 Å thick) to nine Fe bilayers (26 atomic layers, ∼19 Å thick). Compared to the drastic relaxations
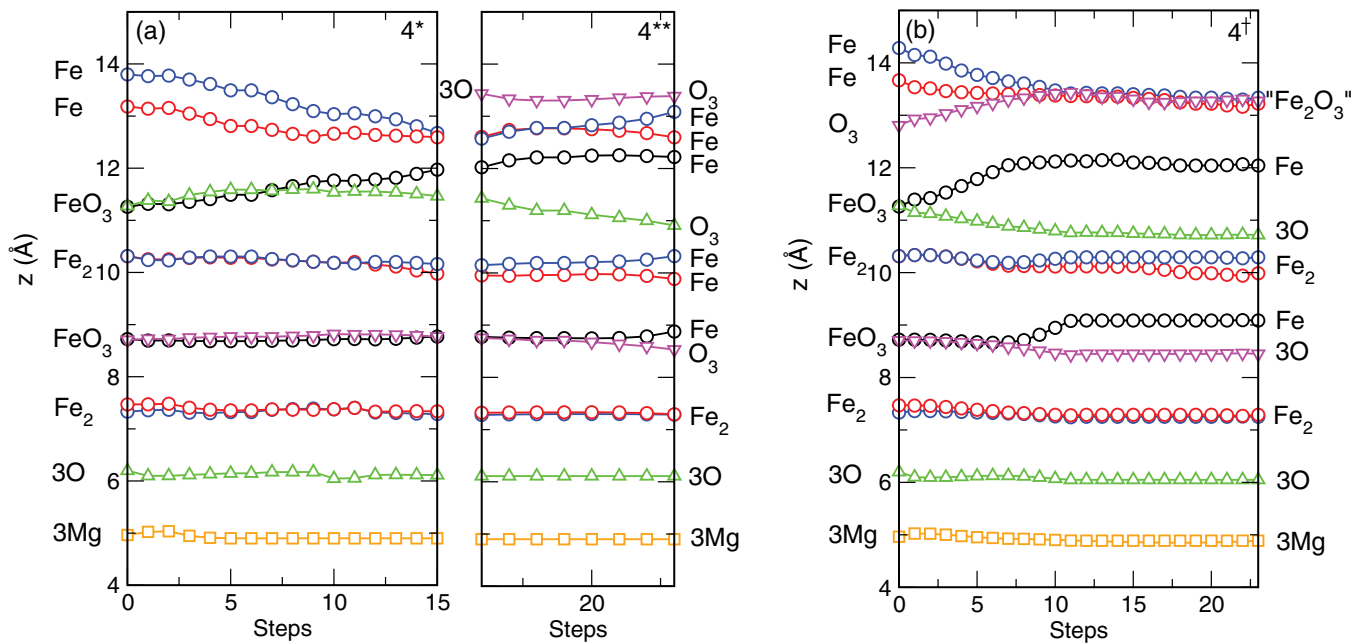
FIG. 4. (Color online) Atomic positions along the surface normal as a function of relaxation step, for an initial geometry consisting of the relaxed three-Fe-bilayers structure of Fig. 3 with a fourth Fe_2O_3 unit added by (a) an Fe bilayer followed by a 3O plane after 15 relaxation steps, or (b) a complete 3(O-Fe-Fe) unit at the start of the calculation. The sequential approach is also more appropriate on the layer-by-layer growth.

found in the heterointerface calculations for hematite films on MgO(111), the inter- and intraplanar relaxations for the equivalent unsupported $Fe_2O_3(0001)$ films are less dramatic and do *not* show the FeO_3-type stacking seen for the interface structures. A common feature of all the free-standing slabs is a strong inward displacement of the Fe bilayer at the surface with a simultaneous outward displacement of the surface oxygen layer, resulting in a contraction of as much as 75% ($\Delta d = 0.5$ Å) in $d_\perp^{Fe-O}$ between the surface Fe and O layers, a natural response of the system to the absence of neighbors at the surface. Note that while the interlayer contractions (expansions) are large, the changes in the bond lengths are far more modest, with contraction in nearest-neighbor Fe-Fe and Fe-O bond lengths of $\sim$7% and 2%, respectively. For thinner slabs with three and five Fe bilayers (eight and 14 atomic layers respectively), surface relaxations affect even the deeper layers, manifested by the collapse of the Fe bilayer at the center to a nearly coplanar layer, i.e., $d_\perp^{Fe-Fe} \sim 0$ at the center of the film. Such an effect is not observed in thicker slabs (>five Fe bilayers) where the deeper layers maintain almost bulklike intra- and interlayer distances; the contraction in the intralayer Fe-Fe separation is $\sim$0.02 Å. The five-Fe-bilayer film shows much larger relaxations than the other structures and represents a transition between ultrathin and thin (bulklike) unsupported hematite films.

Since the Fe_2O_3-MgO supercells used the in-plane lattice constant of the MgO(111) substrate, which is $\sim$0.098 Å (3%) larger than the bulk Fe_2O_3 lattice constant, the question arises whether the unexpected relaxations in the film are the result of the lattice mismatch between the MgO substrate and the hematite film. Calculations of unsupported hematite slabs at the larger MgO lattice constant

show relaxations and magnetic ordering similar to those using the bulk hematite constant, indicating that the unusual behavior of the Fe_2O_3 film on MgO is related to the (polar) interface.

Free-standing $Fe_2O_3(0001)$ slabs initiated with two $Fe_2|FeO_3$ surface layers (using the heterointerface results as a starting point) on bulk Fe_2O_3 unit are structurally unstable. The final relaxed structure, however, does not have the normal bulk ...3O|Fe-Fe|3O|Fe-Fe geometry, but rather ...3O|Fe-Fe_2|3O|Fe_2|3O|Fe. This structure, which is higher in energy (by $\sim$0.14 eV/surface) than the $Fe_2O_3(0001)$ slab structures described earlier, shows a monolayer Fe termination arising from the breakup of the top FeO_3 layer. The other FeO_3 layer likewise decomposes, resulting in a combination of a "bilayer" of Fe and an Fe_2 plane. Such striking differences between the atomic structures of relaxed $Fe_2O_3(0001)$ slabs and $Fe_2O_3(0001)$ films on polar MgO(111) suggest that the structural relaxations are a response of the film to the interface polarity and a possible way of minimizing it.

Further evidence of the effect of the heterointerface polarity on the structure of hematite films is obtained from calculations of $Fe_2O_3(0001)$ films on metallic Ti(0001) substrates. Ti has an in-plane lattice constant ($a_{hex} = 2.6$ Å) $\sim$2.6% larger than hematite. As opposed to the case of the polar heterointerface, the stacking sequence of a three-bilayers hematite film on Ti remains bulklike in structure with metallic states throughout the film, again pointing to the role of the polarity of the interface.

B. Magnetic structure

A search over a broad range of spin-configuration space found a number of thickness-dependent metastable spin states (cf. Table IV) for the interface systems. For the initial growth

TABLE IV. Stable local spin configurations of the $Fe_2O_3(0001)/MgO(111)$ heterointerfaces for different hematite film thicknesses. Up and down spins are indicated by $+$ and $-$, respectively. For the $n = 3$ case, there are four, rather than three, Fe layers because of the relaxations.

No. of Fe bilayers	Local spin structure
1	$0\| + +$
2	$0\| + -\| - +$
3	$0\| + -\| -\| + -\|-$
4	$0\| + +\| - -\| + +\| - +$

of one Fe bilayer ($n = 1$), the FM $++$ interface is found to be energetically favorable compared to the AF $+-$ interface by ~ 0.22 eV/interface. Both spin configurations have a metallic interface. Of the various possible models for the supercell with $n = 2$ Fe bilayers, the AF_I ($+ - | - +$) interface is found to be lowest in energy, with the bulklike AF_B $++|--$ interface higher in energy by ~ 0.1 eV/interface, and the FM model still much higher in energy.

Because the relaxed $n = 3$ Fe-bilayer film no longer has the well-defined bilayer structure, the magnetic ordering is necessarily different in character. In this case, there are now four Fe layers, and the ordering can be written as $+ - | - | + -|-$, where the single moments are for the FeO_3 layers. The two Fe_2 are antiferromagnetically coupled within the layer and ferromagnetically between. Similarly, the two FeO_3 planes are coupled ferromagnetically. The calculated magnetic moments in the Fe spheres are smaller, ~ 3.0–$3.2 \mu_B$, for the Fe atoms near the surface compared to the bulk Fe_2O_3 value of $\sim 3.4 \mu_B$. With the addition of another bilayer ($n = 4$), the magnetic structure reverts to the bulklike configuration, except at the surface.

Unsupported $Fe_2O_3(0001)$ slabs also show thickness-dependent magnetic properties. Comparison of the calculated total energies for the AF_B, AF_I ($+ - | - +$), and AF_{II} ($+ - | + -$) spin configurations show that for thinner films (three and five Fe bilayers), the energetically favorable structure corresponds to AF_I ordering throughout the film. For thicker slabs, the surface bilayer has an AF_I spin arrangement (antiparallel moments within the surface bilayer), whereas the deeper layers have the bulklike AF_B arrangement. Because of the presence of energy barriers between these (meta)stable states, earlier studies of hematite surfaces[20,22,23] found the bulklike orderings only. The transition region for unsupported polar $Fe_2O_3(0001)$ is about five Fe bilayers (14 atomic layers), i.e., one recovers bulk behavior in slabs thicker than approximately five bilayers, while thinner slabs have significant structural and magnetic differences compared to bulk hematite.

C. Correlations and structural properties

As noted earlier, the iron oxides are generally considered to be correlated electron systems. Although the structural properties of bulk Fe_2O_3 calculated using either GGA or GGA $+ U$ are quite similar—largely because both yield AFM insulators—it is not obvious that the same will hold true for the polar interface system, or what value of U would be appropriate. In the spirit of treating the Hubbard U as a model parameter, we have investigated what effect inclusion of U has on both the structural parameters and the eigenvalue spectra for the relaxed three-bilayer structure.

The relaxed GGA and GGA $+ U$ structures are shown in Fig. 5 for $U - J = 4$ eV. (For $U - J < 2$ eV, the structure is essentially the same as the GGA one.) The FeO_3 does unfold slightly in the GGA $+ U$ calculations, where the largest change is that the Fe in the surface FeO_3 layer moves outward by about 0.45 Å. Despite this change, the GGA $+ U$ structure does not revert to the bulklike stacking, but instead retains the main aspects of the GGA interface structure, namely, the collapse of the Fe bilayers and the FeO_3 layer near the interface. Although we have not repeated the full layer-by-layer process for GGA $+ U$, the results show that the GGA structure is at least metastable when electron correlations at the GGA $+ U$ level are included.

The effect of GGA $+ U$ on the density of states (Fig. 5) is more dramatic. For the Fe local density of states (LDOS), the spectral weight of the majority (minority) $3d$ states is pushed to deeper (higher) energies; the shifts in the O LDOS are mainly a reflection of these changes. For the collapsed Fe bilayers, Fe_{S-3} and Fe_{S-1}, this shift is so large that split-off states are formed below the bottom of the bands, an indication that $U - J = 4$ eV is too large a value for these atomic sites, but might be reasonable for the FeO_3 and "Fe $+ O_3$" sites. These results strongly indicate that different U values are needed for the different sites, but what the appropriate values might be is unknown; we cannot use the standard approach of matching band gaps to choose U since there are no (site-resolved) experimental electron spectroscopy results for this interface system.

With the caveat that the choice of U overestimates the effect of correlations in at least parts of the film, we note that both the GGA and GGA $+ U$ give half-metallic behavior throughout the film, although the DOS at the Fermi level is much reduced for the GGA $+ U$ calculations due mainly to sharp states at E_F. Scanning tunneling microscopy provides a possible experimental technique to probe these electronic states.

D. Coulomb potentials and core-level shifts (CLSs)

Since the self-consistent planar-averaged Coulomb potential $V_c(z)$ implicitly includes the contributions from both quantum mechanical screening and structural changes, it provides a physical basis for discussing polarity (uncompensated dipole) effects if they exist.[40–43] Figure 6(a) shows the calculated (solid) and fitted (dashed) planar-averaged Coulomb potential, while Fig. 6(b) gives the corresponding ionic potential for the relaxed three-bilayer system. The results of the fitting are given in Table V. The calculated and fitted potentials agree very well, with the exception in the very near surface region. (This expected discrepancy[44] in the surface dipole is caused by changes in the tails of the electron wave functions at the surface that are not well described by the atomiclike tails of the overlapping densities; an additional fitting parameter could be included to account for this effect, but it would not alter the conclusions of this analysis.)
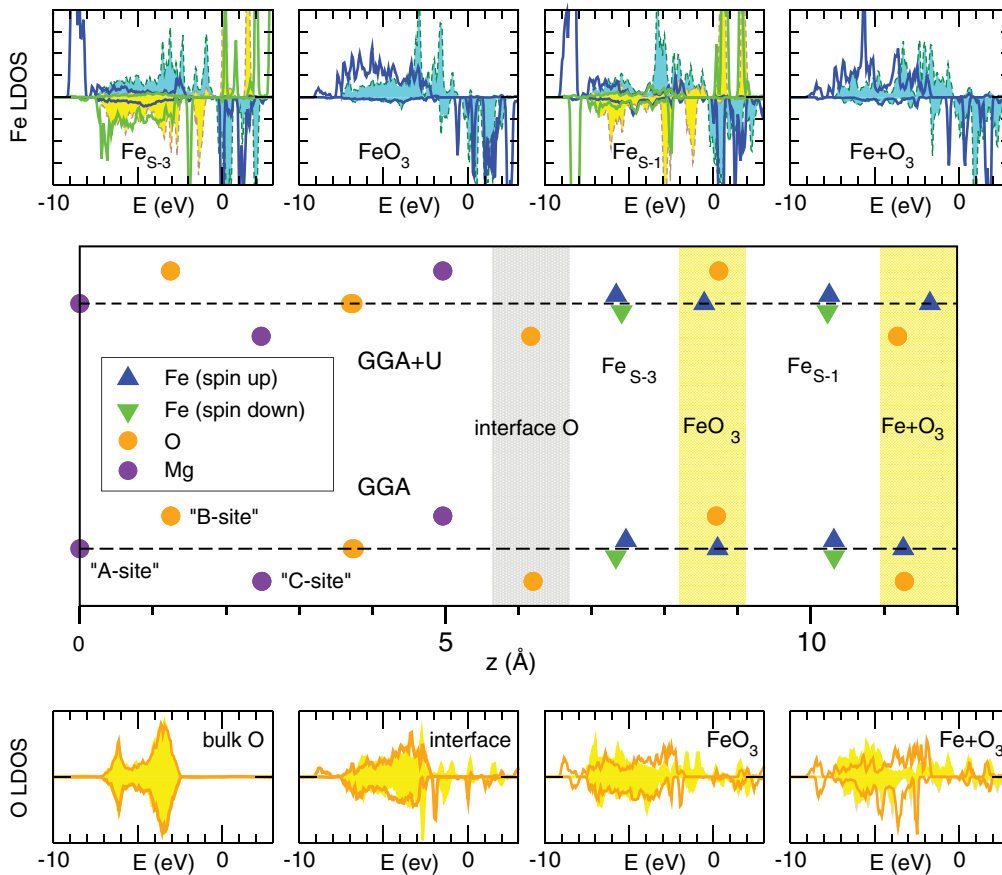
FIG. 5. (Color online) Comparison of the planar positions of the GGA and GGA $+ U$ ($U - J = 4$ eV) relaxed three-bilayer structures. The positions relative to the dotted lines represent the stacking sites; atomic sites are labeled according to their positions in the film. The Fe and O spin-resolved local density of states for the different atoms are shown in the top and bottom panels; the GGA results are given as filled regions while the GGA $+ U$ results are given as solid lines.

As is evident from the oscillating nature of the ionic potential, the MgO(111) substrate is ionic, with each ion having a net fitted charge of about ± 0.36, rather than the nominal charges of ± 2. Also evident from the plot of the ionic potential is that there is a shift in the average ionic potential (V_{av}) as one goes across the interface between the two regions. This dipole potential shift is plotted in Fig. 6(c) as a function of the number of Fe bilayers in the film for both the relaxed and unrelaxed structures. The simple classical expectation of a growing dipole potential difference with increasing thickness of a polar film is clearly not supported by the calculations. For all thicknesses (except $n = 2$), the potential in the relaxed films is lower than that in the structurally unrelaxed film. The drastic structural relaxations in the three-Fe-bilayers film cause a sharp drop in the potential shift, i.e., the screening of the dipole field due to structural relaxations is concomitant with the overall stabilization of the heterointerface. As discussed in Sec. III A, films with four Fe bilayers were modeled starting with the typical Fe_2O_3 stacking (solid symbols) and also starting from the relaxed structure of three Fe bilayers and an Fe-Fe|O_3 unit (hashed symbols). Even though the relaxed structures have different end points due to the presence of an energy barrier of ~ 0.14 eV, the net effect of the electronic and structural relaxation is a lowering of the dipole in both cases.

The values of the charges for the unrelaxed and the relaxed three-Fe-bilayers film on MgO(111) given in Table V give further evidence that the structural relaxations and the minimization of polarity are related. For both the unrelaxed and relaxed structures, the interfacial O is more ionic than in MgO; for the unrelaxed film, the ionicity is similar to that in the Fe_2O_3 film, but for the relaxed structure it is increased by $\sim 10\%$. Conversely, structural relaxation reduces the ionicity of Fe_2 layers, as well as that of the FeO_3 layers compared to the unrelaxed structure. Thus, the interfacial oxygen layer plays a major role in the electronic screening of the MgO dipole field, whereas the structural relaxations in the hematite film act to reduce the ionicity of the film.

The shifts in the Coulomb potential should be accessible experimentally through the measurement of core-level binding energy shifts (CLSs). The calculated initial state (i.e., neglecting the core-hole effects) O $1s$ CLSs for the two FeO_3 layers in the $n = 3$ film are shifted by -1.15 and -1.05 eV (to greater binding energy) compared to that of the MgO substrate, while there is a shift of -0.15 eV for the oxygen layer at the interface. The similarity of the shifts in the FeO_3 planes are a result of the fact that the intra- and interlayer contributions are almost identical for the two FeO_3 layers. An analysis[45] of the interatomic charge transfer (the change in charge contained
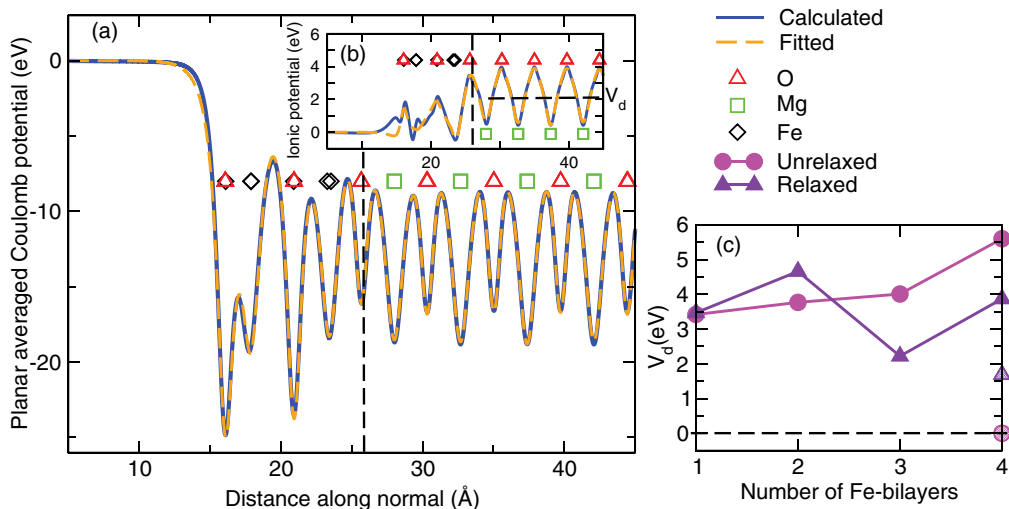
FIG. 6. (Color online) Planar-averaged (a) Coulomb and (b) ionic potential for calculated (solid) and fitted (dashed) charges for the relaxed three-Fe-bilayers-thick $Fe_2O_3(0001)$ film on MgO(111). Positions of Fe (diamond), O (triangle), and Mg (square) atoms are also shown. (c) Dipole potentials across the unrelaxed (solid circle) and relaxed (solid triangle) hematite films as a function of the number of Fe bilayers. The hashed circle and triangle show the dipole potentials for an unrelaxed and relaxed four-Fe-bilayers film, respectively, initiated with an O_3 termination. The dipole potential V_d is calculated as the difference between the average ionic potential in the MgO substrate and the vacuum zero.

in the atomic sphere) and charge redistribution (change in the shape of wave function) shows that these two factors have negligible contribution to the core-level shifts, implying that the contributions from extra-atomic terms are dominant. Moreover, the ionic charges in Table V show that the FeO_3 layers act as though they are approximately neutral. For comparison, for the initial (unrelaxed) hematite film structure on MgO, the oxygen plane nearest the surface has a shift of 1.31 eV, the next oxygen plane is less binding by 0.45 eV, and the CLS at the interface is -0.26 eV. These larger variations in the CLS result from the presence of the surface and the more ionic bonding in hematite compared to the relaxed structure. [For the nine-bilayer $Fe_2O_3(0001)$ slab, the oxygen plane nearest (next nearest) the surface of the has a CLS of -0.8 (-0.2) eV.]

IV. CONCLUSIONS

We have presented a first-principles study of the atomic, electronic, and magnetic structure of the polar $Fe_2O_3(0001)$/MgO(111) heterointerface. Model calculations for the layer-by-layer growth of polar hematite films on polar magnesia substrates show the interface is oxidelike and atomically abrupt, suggesting that intermixing at the interface is not a dominant stabilization mechanism for this system. The polarity of the interface has a marked effect on the growth of the films in that it results in drastic structural relaxations, especially at a film thickness of three bilayers. Large motions of Fe and O atoms in the film lead to the formation of an $Fe_2|FeO_3$ stacking which does not exist in any of the naturally occurring bulk iron oxides. Our calculations show the presence

TABLE V. Least-squares-fitted ionic charges for unrelaxed and relaxed three-Fe-bilayers-thick $Fe_2O_3(0001)$ film on MgO(111) substrate. Net charge is given in e^- per planar unit cell. When atomic planes are (approximately) degenerate, only the sum of charges can be determined, not the individual ones.

Three Fe bilayers	Unrelaxed			Relaxed		
	Atomic plane	Charge	Charge/ion	Atomic Plane	Charge	Charge/ion
Film	Fe-Fe	0.60	0.20, 0.40			
	3O	-1.23	-0.41	FeO_3	-0.09	
	Fe-Fe	1.25	0.67, 0.58	Fe_2	0.29	
	3O	-1.23	-0.41	FeO_3	-0.38	
	Fe-Fe	1.39	0.60, 0.79	Fe_2	1.04	
Interface	3O	-1.26	-0.42	3O	-1.38	-0.46
Substrate	3Mg	1.02	0.34	3Mg	1.05	0.35
	3O	-1.08	-0.36	3O	-1.05	-0.35
	3Mg	1.08	0.36	3Mg	1.05	0.35
	3O	-1.08	-0.36	3O	-1.08	-0.36
	3Mg	1.08	0.36	3Mg	1.05	0.35

of different local minima for films starting from different initial conditions and the importance of both experimental conditions and the layer-by-layer modeling of the growth. Thus, layer-by-layer epitaxial growth of such polar interfaces allows for the synthesis of metastable states with unique structural, electronic, and magnetic properties that do not exist in the bulk phases. Within the GGA, the thinnest film with one Fe bilayer is found to be metallic, while those with two, three, and four Fe bilayers are half metallic throughout the film. The effect of inclusion of Hubbard U on the structural parameters shows that for $U - J < 2$ eV, the structure remains essentially unchanged, while for $U - J = 4$ eV, a value appropriate for bulk Fe_2O_3, there is a some unfolding of the FeO_3 planes, but the GGA $+ U$ structure does not revert to the bulklike stacking. The effect of GGA $+ U$ is most pronounced in the Fe $3d$ LDOS. For $U - J = 4$ eV, the formation of split-off states in the collapsed Fe_2 planes indicate that this value of U is too large for Fe, but reasonable for the FeO_3 sites,

i.e., there is not a single unique value of U appropriate for all the different sites in the film. Analysis of the Coulomb potential shows a sharp drop in the dipole potential in the three-Fe-bilayers film, suggesting that the stabilization of the polar interface and screening of the dipole field occur due to the combined effect of electronic and structural relaxations in the heterointerface.

[1] J. Goniakowski, F. Finocchi, and C. Noguera, Rep. Prog. Phys. **71**, 016501 (2008).

[2] E. Dagotto, Science **318**, 1076 (2007).

[3] J. Chakhalian, J. W. Freeland, H.-U. Habermeier, G. Christiani, G. K. M. van Veenendaal, and B. Keimer, Science **318**, 1114 (2007).

[4] W. Luo, S. J. Pennycook, and S. T. Pantelides, Phys. Rev. Lett. **101**, 247204 (2008).

[5] A. Brinkman, M. Huijben, M. V. Zalk, J. Huijben, U. Zeitler, J. C. Maan, W. G. van der Wiel, G. Rijnders, D. H. A. Blank, and H. Hilgenkamp, Nat. Mater. **6**, 493 (2007).

[6] N. Reyren, S. Thiel, A. D. Caviglia, L. F. Kourkoutis, G. Hammerl, C. Richter, C. W. Schneider, T. Kopp, A.-S. Ruetschi, D. Jaccard, M. Gabay, D. A. Muller, J.-M. Triscone, and J. Mannhart, Science **317**, 1196 (2007).

[7] A. Kalabukhov, R. Gunnarsson, J. Borjesson, E. Olsson, T. Claeson, and D. Winkler, Phys. Rev. B **75**, 121404(R) (2007).

[8] M. Basletic, J.-L. Maurice, C. Carretero, G. Herranz, O. Copie, M. Bibes, E. Jacquet, K. Bouzehouane, S. Fusil, and A. Barthelemy, Nat. Mater. **7**, 621 (2008).

[9] R. Pentcheva and W. E. Pickett, Phys. Rev. Lett. **102**, 107602 (2009).

[10] N. Nakagawa, H. Y. Hwang, and D. A. Muller, Nat. Mater. **2**, 204 (2006).

[11] A. Ohtomo and H. Y. Hwang, Nature (London) **427**, 423 (2004).

[12] R. M. Cornell and U. Schwertmann, *The Iron Oxides: Structure, Properties, Reactions, Occurrences and Uses* (Wiley-VCH, Weinheim, 2003).

[13] V. K. Lazarov, S. A. Chambers, and M. Gajdardziska-Josifovska, Phys. Rev. Lett. **90**, 216108 (2003).

[14] W. Weiss, A. Barbieri, M. A. Van Hove, and G. A. Somorjai, Phys. Rev. Lett. **71**, 1848 (1993).

[15] V. K. Lazarov, M. Weinert, S. A. Chambers, and M. Gajdardziska-Josifovska, Phys. Rev. B **72**, 195401 (2005).

[16] M. Catti, G. Valerio, and R. Dovesi, Phys. Rev. B **51**, 7441 (1995).

[17] L. M. Sandratskii, M. Uhl, and J. Kübler, J. Phys.: Condens. Matter **8**, 983 (1996).

[18] M. P. J. Punkkinen, K. Kokko, W. Hergert, and I, J. Väyrynen, J. Phys.: Condens. Matter **11**, 2341 (1999).

[19] G. Rollmann, A. Rohrbach, P. Entel, and J. Hafner, Phys. Rev. B **69**, 165107 (2004).

[20] X.-G. Wang, W. Weiss, S. K. Shaikhutdinov, M. Ritter, M. Petersen, F. Wagner, R. Schlögl, and M. Scheffler, Phys. Rev. Lett. **81**, 1038 (1998).

[21] W. Weiss and W. Ranke, Surf. Sci. **70**, 1 (2002).

[22] A. Rohrbach, J. Hafner, and G. Kresse, Phys. Rev. B **70**, 125426 (2004).

[23] W. Bergermayer, H. Schweiger, and E. Wimmer, Phys. Rev. B **69**, 195409 (2004).

[24] E. Wimmer, H. Krakauer, M. Weinert, and A. J. Freeman, Phys. Rev. B **24**, 864 (1981).

[25] M. Weinert, E. Wimmer, and A. J. Freeman, Phys. Rev. B **26**, 4571 (1982).

[26] M. Weinert, G. Schneider, R. Podloucky, and J. Redinger, J. Phys.: Condens. Matter **21**, 084201 (2008); [http://www.uwm.edu/weinert/flair.html].

[27] J. P. Perdew, K. Burke, and M. Ernzerhof, Phys. Rev. Lett. **77**, 3865 (1996).

[28] W. A. Harrison, E. A. Kraut, J. R. Waldrop, and R. W. Grant, Phys. Rev. B **18**, 4402 (1978).

[29] S. H. Cheung, A. Celik-Aktas, P. Dey, K. Pande, M. Weinert, B. Kabius, D. J. Keavney, V. K. Lazarov, S. A. Chambers, and M. Gajdardziska-Josifovska, Phys. Rev. B **85**, 045405 (2012).

[30] S. Gota, E. Guiot, M. Henriot, and M. Gautier-Soyer, Phys. Rev. B **60**, 14387 (1999).

[31] B. Handke, J. B. Simonsen, M. Bech, Z. Li, and P. J. Møller, Surf. Sci. **600**, 5123 (2006).

[32] M. Lübbe, A. M. Gigler, R. W. Stark, and W. Moritz, Surf. Sci. **604**, 679 (2010).

[33] E. Popova, B. Warot-Fonrose, F. Bonell, S. Andrieu, Y. Dumont, B. Berini, A. Fouchet, and N. Keller, Surf. Sci. **605**, 1043 (2011).

[34] M. Ritter, H. Over, and W. Weiss, Surf. Sci. **371**, 245 (1997).

[35] C. Schlueter, M. Lübbe, A. M. Gigler, and W. Mortiz, Surf. Sci. **605**, 1986 (2011).

[36] M. Xue, S. Wang, K. Wu, J. Guo, and Q. Guo, Langmuir **27**, 11 (2011).

[37] D. Telesca, B. Sinkovic, S.-H. Yang, and S. S. P. Parkin, J. Electron. Spectrosc. Relat. Phenom. (2012), doi: 10.1016/j.elspec.2012.04.002.

[38] S. A. Chambers and S. I. Yi, Surf. Sci. Lett. **439**, L785 (1999).

[39] A. Barbier, A. Stierle, F. Finocchi, and J. Jupille, J. Phys.: Condens. Matter **20**, 184014 (2008).

[40] V. K. Lazarov, Ph.D. thesis, University of Wisconsin, Milwaukee, 2005.

[41] V. K. Lazarov, J. Zimmerman, S. H. Cheung, L. Li, M. Weinert, and M. Gajdardziska-Josifovska, Phys. Rev. Lett. **94**, 216101 (2005).

[42] J. Goniakowski, C. Noguera, and L. Giordano, Phys. Rev. Lett. **98**, 205701 (2007).

[43] V. K. Lazarov, M. Weinert, and M. Gajdardziska-Josifovska (unpublished).

[44] M. Weinert and R. E. Watson, Phys. Rev. B **29**, 3001 (1984).

[45] M. Weinert and R. E. Watson, Phys. Rev. B **51**, 17168 (1995).